

**Formation of spin droplet at  $\nu = \frac{5}{2}$  in an asymmetric quantum dot under quantum Hall conditions**H. Atci<sup>1,2,\*</sup> and A. Siddiki<sup>3</sup><sup>1</sup>*Department of Physics, ETH Zurich, CH-8093 Zurich, Switzerland*<sup>2</sup>*Physics Department, Istanbul University, 34134 Vezneciler-Fatih, Istanbul, Turkey*<sup>3</sup>*Physics Department, Mimar Sinan Fine Arts University, 34380 Bomonti-Sisli, Istanbul, Turkey*

(Received 30 September 2016; revised manuscript received 30 November 2016; published 19 January 2017)

In this work, a quantum dot that is defined asymmetrically by electrostatic means induced on a GaAs/AlGaAs heterostructure is investigated to unravel the effect of geometric constraints on the formation of spin droplets under quantized Hall conditions. The incompressibility of the excited  $\nu = \frac{5}{2}$  state is explored by solving the Schrödinger equation within spin density functional theory, where the confinement potential is obtained self-consistently utilizing the Thomas-Fermi approximation. Our numerical investigations show that the spatial distribution of the  $\nu = 2$  incompressible strips and electron occupation in the second lowest Landau level considerably differ from the results of the laterally symmetric quantum dots. Our findings yield two important consequences: first, the incompressibility of the intriguing  $\nu = \frac{5}{2}$  state is strongly affected by the asymmetry, and second, since the Aharonov-Bohm interference patterns depend on the velocity of the particles, asymmetry yields an additional parameter to adjust the oscillation period, which imposes a boundary condition dependency in observing quasiparticle phases.

DOI: [10.1103/PhysRevB.95.045132](https://doi.org/10.1103/PhysRevB.95.045132)**I. INTRODUCTION**

The fractional quantum Hall states assuming an even-denominator Landau level (LL) filling factor [1] have recently come into the limelight both in experimental [2–6] and theoretical investigations [7–9] due to a theoretical prediction that they are promising candidates to be useful for topological quantum computing [10]. The use of topological charge is constrained by the measurements, which should be able to read out the qubits. Hence, interferometers are indispensable for the implementation of topological quantum computation. The topological quantum computation proposal seeks to explore quasiparticle statistics of a particular fractional quantum Hall state, namely filling factor  $\nu = \frac{5}{2}$ , which is believed to obey non-Abelian statistics [11]. Theoretical investigations based on the analysis of composite fermions suggest a  $p$ -wave paired state, described by a Moore-Read-Pfaffian wave function, as a trial wave function for the ground state at filling factor  $\nu = \frac{5}{2}$ . Experimental investigation of the non-Abelian statistics of the  $\nu = \frac{5}{2}$  fractional quantum Hall state can be performed by Fabry-Perot interferometry (FPI) of quasiparticles, leaning on the Aharonov-Bohm (AB) phase [12,13]. Recently, there have been advances in realizing quantum Hall edge-state based interferometers at fractional filling factors at the lowest LL [14,15]. Much of the attention has been focused on the filling factor  $\nu = \frac{5}{2}$  state in quantum dots (QDs) which consist of the two LLs [16–18]. For an infinite system the lowest LL is fully occupied and is spin compensated, whereas the second lowest LL is spin polarized. For a finite system, e.g., a QD, the formation of a spin droplet (SD) is expected, due to competition between the confinement potential and interactions. Once the spin-polarized electrons in the second lowest LL are localized to the center of the QD emanating from exchange-correlation effects, they are called SDs, which are many-body phenomena of interacting electrons [16,19,20].

Rasanen *et al.* [16] showed theoretical evidence of SD formation in large ( $N \geq 30$ ) QDs at the filling factor range  $2 < \nu < 3$  by using numerical many-electron methods. Their calculations indicate that the paired electron state breaks down leading to fragmentation of spin and charge densities in parabolic external confining potentials. They point out that evidence of the fragmentation can be tested by investigating the spatial dependence of the spin and charge densities in different geometries. Our previous work [17] was a systematic investigation of the stability of SDs at the filling factor range  $2 < \nu < 3$  considering broken rotational symmetry. There it was shown that the broken rotational symmetry does not considerably affect the stability of SD formation. However, the stability of a SD under complete breakdown of both the axial and the rotational symmetry of the confinement is still under debate and such an asymmetric confinement is much more realistic in investigating experimental systems. Here, we perform numerical investigation of the formation of SDs in a half-side etched, half-side gated QD yielding an asymmetric confining potential.

We should clarify that in mesoscopic ( $R \geq 10 \mu\text{m}$ ,  $R$  being the radius of quantum dot) and macroscopic ( $R \sim 1 \text{ mm}$ ) devices, both the integer quantum Hall effect and fractional quantum Hall effect are essentially described by bulk properties, i.e., by nonlocal many-body wave functions (e.g., Laughlin  $1/3$  state [21]). These fractional quantum Hall states emerge from topological phase protection. However, once the edge effects, namely the physical boundaries, are taken into account and the number of particles is in the more-than-a-few regime ( $N \sim 10\text{--}100$ ), calculating the local (spatial) electron or composite-Fermion distribution becomes important. In our work, we are in this regime, where  $R$  is less than 500 nm lithographically. Moreover, due to the electrostatic repulsion emanating from the gates/trenched-gates the particles are trapped in an effective dot with a radius of  $\sim 220 \text{ nm}$ .

The outline of this paper is as follows. In Sec. II we briefly describe the GaAs/AlGaAs heterostructure and introduce confinement potential of the device with a self-consistent

\*huseyinatci@gmail.com

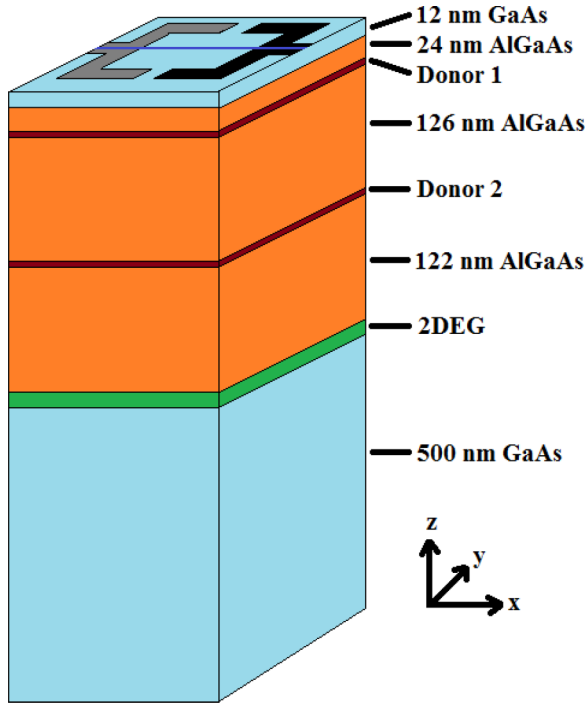


FIG. 1. Sketch of the layer sequence of GaAs/AlGaAs heterostructure, which has the dimensions of  $2550 \times 2550 \times 784 \text{ nm}^3$ . The heterostructure is grown on a thick GaAs substrate, where 2DEG is formed at the interface of the GaAs/AlGaAs denoted by the green region. Silicon donor layers (dark brown regions), distributed homogeneously on the  $xy$  plane, provide electrons both to the surface and to the 2DEG. The light gray and black regions on the surface are shown as the etched and the metallic gate regions, respectively.

electronic calculation. Then we solve computationally the many-electron problem using the spin density functional theory (SDFT). In Sec. III, we analyze the electronic structure of fragmented quantum Hall states and show that the incompressibility of the  $\nu = \frac{5}{2}$  state is affected by the asymmetry. In Sec. IV we conclude our work with discussion of the relevance of our findings to formation of the spin droplet at the filling factor  $\nu = \frac{5}{2}$  quantum Hall state in a confined two-dimensional electron gas (2DEG). The paper is summarized in Sec. V.

## II. THE GEOMETRY AND MODEL HAMILTONIAN

The system we study is shown in Fig. 1; a GaAs/AlGaAs heterostructure [22,23] consists of two  $\delta$ -doped silicon donor layers (dark brown regions) which provide electrons to the 2DEG (green region) forming 284 nm below the surface at the interface between GaAs and AlGaAs. The donor layers lie 122 nm and 248 nm above the 2DEG and have the surface densities  $2.5 \times 10^{15} \text{ m}^{-2}$  and  $1.7 \times 10^{16} \text{ m}^{-2}$ , respectively. The physical dimensions of the heterostructure are taken as  $L_x = L_y = 2550 \text{ nm}$  via a matrix of  $128 \times 128$  mesh points. The left side of the heterostructure (light gray region) is etched 80 nm below the surface and different voltages are applied to a metallic gate which is deposited on the surface of heterostructure at the right side (black region). The metallic gate is biased with  $-1.8 \text{ V}$ ,  $-2.0 \text{ V}$ ,  $-2.3 \text{ V}$ , and  $-2.9 \text{ V}$ , respectively. The realistic modeling of the 2DEG to

be located at  $z = 0$  relies on solving the Poisson equation in three dimensions self-consistently within the Thomas-Fermi approximation (TFA) which describes realistically the electronic distribution for the given boundary conditions, set by the GaAs/AlGaAs heterostructure and surface patterns. To calculate electron and potential profiles within the TFA the computational effort is much simpler than other quantum mechanical calculations and yields compatible results. The spatial distribution of the electron density is calculated within the TFA [24,25],

$$n_{\text{el}}(x, y) = \int D(E) f[E + V_{\text{tot}}(x, y) - \mu^*] dE \quad (1)$$

with  $D(E) \equiv \sum \delta(E - E_n)$  describing the local density of states (LDOS),  $f(E) = 1/[\exp(E/k_B T) + 1]$  as the Fermi function,  $\mu^*$  as the electrochemical potential,  $k_B$  as the Boltzmann constant, and  $T$  as the temperature. We write the total potential energy of an electron as

$$V_{\text{tot}}(x, y) = V_{\text{ext}}(x, y) + V_{\text{H}}(x, y), \quad (2)$$

where  $V_{\text{ext}}(x, y)$  and  $V_{\text{H}}(x, y)$  are the external (confining) potential composed of gates and donors and the electron-electron interaction (Hartree) potential, respectively. Since the Hartree potential depends on the electron density via [26]

$$V_{\text{H}}(x, y) = \frac{2e^2}{\epsilon} K(x, y, x', y') n_{\text{el}}(x', y') dx' dy', \quad (3)$$

where  $-e$  is the electron charge,  $\epsilon$  is the dielectric constant ( $=12.4$  for GaAs), and the kernel  $K(x, y, x', y')$  is the solution of the 2D Poisson equation with appropriate boundary conditions, Eqs. (1) and (2) complete the self-consistent loop [27], which can be solved by a numerical iteration. This kernel can be found in a well-known textbook [28]. To solve the Poisson equation we use a code developed by Weischelbaum which has successfully been applied in earlier studies [29–32]. Overall the code provides a reliable description of the potential landscape both in the absence and presence of electron-electron interactions in the 2DEG. To obtain the confining potential, we use the half-side etched and half-side gated heterostructure depicted in Fig. 1. In Fig. 2, we show results of the confining potential that is nearly symmetric when  $-2.3 \text{ V}$  is applied to the metallic gate; however the spatial symmetry is lifted for gate voltages  $-1.8 \text{ V}$ ,  $-2.0 \text{ V}$ , and  $-2.9 \text{ V}$ , respectively.

Motivated by the experiments, we investigated the above-mentioned geometry and structure. On one hand, we are not able to judge whether the experiments (Refs. [22,23,33–36]) can describe the full picture of the  $\frac{5}{2}$  state. However, their experimental results coincide; in contrast interpretations strongly differ. On the other hand, the question of whether the observations stem from phase protection (Aharonov-Bohm/Berry) or whether particle interactions (bare Coulomb, exchange, correlation) (Coulomb blockade) dominate the transport is still under debate. Therefore, we think that our investigation which focuses on QDs is valuable for the community. QDs are induced on GaAs/AlGaAs heterostructures confined to a 2D plane and most importantly the electrostatic confinement is spatially asymmetric, under quantum Hall conditions. We use the effective-mass approximation with considering material parameters of a GaAs semiconductor medium, i.e.,

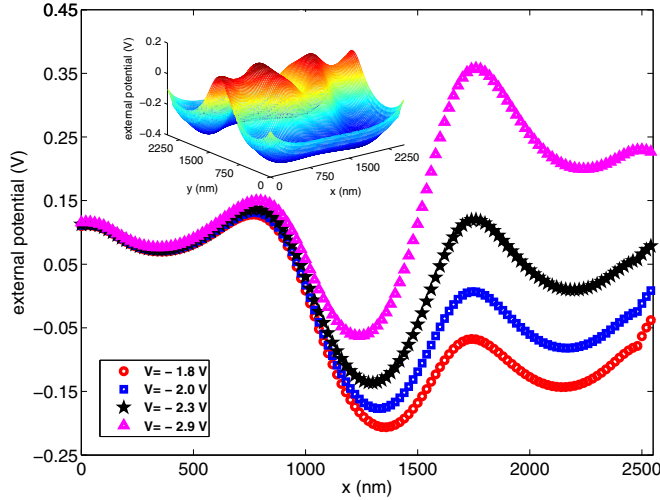


FIG. 2. The confinement potential for electrons at the interface of the GaAs/AlGaAs heterostructure obtained with self-consistent electronic calculations. Inset graph shows the symmetric confinement potential (when applied  $-2.3$  V) more clearly.

the effective mass  $m^* = 0.067m_e$  and the dielectric constant  $\epsilon = 12.4$ . The  $N$ -electron system in an external confining potential and magnetic field is described by an effective-mass Hamiltonian

$$H = \frac{1}{2m^*} \sum_{i=1}^N [-i\hbar\nabla_i + e\mathbf{A}(\mathbf{r}_i)]^2 + \sum_{i<j}^N \frac{e^2}{4\pi\epsilon_0\epsilon|r_i - r_j|} + \sum_{i=1}^N [V_{\text{ext}}(r_i) + g^* \mu_B B S_{z,i}], \quad (4)$$

where  $N$  defines the total electron number inside the quantum dot,  $\mathbf{A} = B/2(-y, x, 0)$  is the vector potential given in the symmetric gauge for the homogeneous magnetic field  $\mathbf{B} = B\hat{z}$  perpendicular to the plane, and  $V_{\text{ext}}(\mathbf{r})$  is the external confining potential in the  $xy$  plane (see Fig. 2). The last term is the Zeeman energy arising from the application of an external magnetic field with electron spin. Here,  $g^* = -0.44$  is the effective gyro-magnetic ratio,  $\mu_B = e\hbar/2m_e$  is the Bohr magneton, and  $S_z = \pm\frac{1}{2}$  represents the up and down spins, respectively. We solve the Schrödinger equation,  $H\Psi = E\Psi$ , associated with the  $N$ -electron Hamiltonian in Eq. (4) using numerical approaches, namely the SDFT in the self-consistent Kohn-Sham formulation [37]. To obtain the ground state energy depends on spin densities  $\sigma = n_\uparrow(\mathbf{r}), n_\downarrow(\mathbf{r})$  of a system of interacting electrons; the Kohn-Sham states are solved from the Kohn-Sham equation [38]

$$[T_0^\sigma + V_{\text{KS}}^\sigma(\mathbf{r})]\varphi_{i\sigma}(\mathbf{r}) = E_{i\sigma}\varphi_{i\sigma}(\mathbf{r}). \quad (5)$$

Here, the first term is the kinetic energy functional of noninteracting electrons with spin densities and the second term is the Kohn-Sham potential  $V_{\text{KS}}^\sigma(\mathbf{r})$ , defined as

$$V_{\text{KS}}^\sigma(\mathbf{r}) = V_{\text{ext}}^\sigma(\mathbf{r}) + V_{\text{H}}^\sigma(\mathbf{r}) + V_{\text{xc}}^\sigma(\mathbf{r}), \quad (6)$$

where the sum of the external confining potential  $V_{\text{ext}}^\sigma(\mathbf{r})$  acting on the interacting system, the classic electrostatic or Hartree potential  $V_{\text{H}}^\sigma(\mathbf{r})$ , and the exchange-correlation potential given

by

$$V_{\text{xc}}^\sigma(\mathbf{r}) = \frac{\delta E_{\text{xc}}^{\text{LSDA}}}{\delta n^\sigma(\mathbf{r})} = \int d\mathbf{r}' n(\mathbf{r}') e_{\text{xc}}(n(\mathbf{r}'), \zeta(\mathbf{r}')), \quad (7)$$

where  $e_{\text{xc}}$  is the exchange-correlation energy per electron, depends on the total spin density  $n = n_\uparrow + n_\downarrow$  and spin polarization  $\zeta = (n_\uparrow - n_\downarrow)/n$ . To calculate exchange-correlation energy  $E_{\text{xc}}$ , we use the local spin density approximation (LSDA) with a parametrization provided by Attaccalite *et al.* [39]. The SDFT scheme together with LSDA leads to good numerical accuracy and produces reliable results in comparison with quantum Monte Carlo calculations in quantum dot systems [16,20,33]. In the SDFT calculations, we utilize the OCTOPUS [40,41] code package (published under the General Public License) built on the real space grid discretization method which allows realistic modeling of two-dimensional systems. Related technical details can be found in Refs. [40,41]. To solve the Schrödinger equation the conjugated gradient algorithm is used.

We point out that for the  $\nu \geq 1$  regime the filling factor can be defined  $\nu = 2N/N_{\text{OLL}}$ , approximately in the QDs. Here,  $N_{\text{OLL}}$  is the number of electrons in the lowest LL. Theoretical investigation of many-body effects in a realistic QD involves the self-consistent solution of the Schrödinger equation. To address the many-body problem, we use SDFT with LSDA [42].

### III. INCOMPRESSIBILITY

Interference phenomena in the quantum Hall regime characterized by strong electron-electron interactions is a very prominent topic in transport [22,34,35]. To investigate interference effects at the edge of the quantum Hall system a type of FPI can be addressed. The novel geometry called FPI which shows edge channels (yellow lines) is shown Fig. 3. Interference occur when current-carrying two-edge channels are at close proximity allowing scattering to provide partitioning. The current-carrying edge channels in the FPI acquire a phase determined by the AB effect and the number

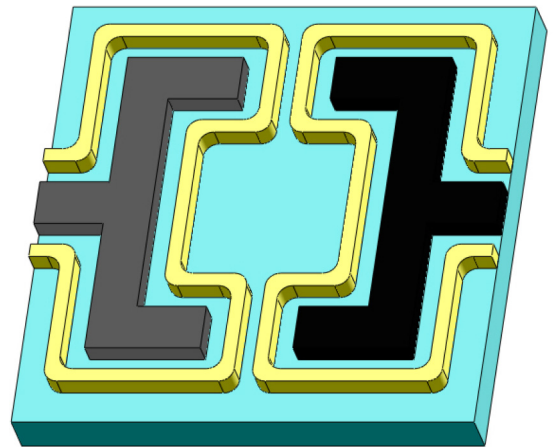


FIG. 3. A FPI device. Current flows along the counterpropagating edge states (shown by yellow lines). Tunneling occurs in the two narrow constrictions, when the edge channels are at a sufficient proximity.

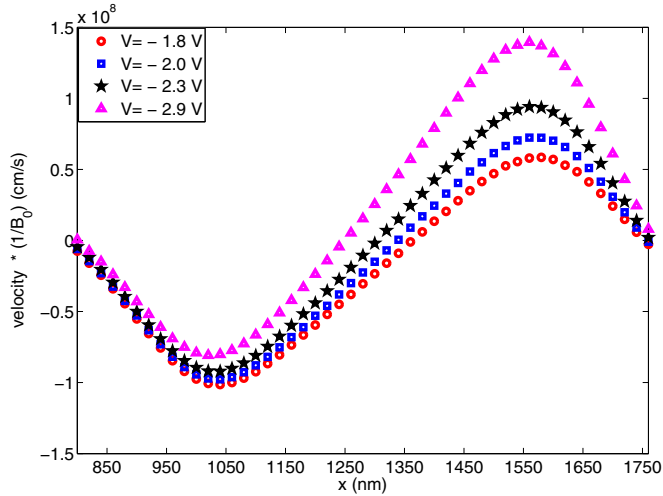


FIG. 4. The slopes of the confinement potential of the sample give the electron velocity as a function of the position.

of quasiparticles. This resultant phase arises from different velocities of the quasiparticles on different paths and can be controlled by either changing the magnetic field or the area of the interferometer [36]. The phase difference is strongly affected by the electron velocity and is an important transport parameter for interferometers. To determine the edge channel velocity in the quantum Hall regime McClure *et al.* [36] used interference to explain checkerboard patterns at a FPI geometry. Using the gradient of the confining potential it is straightforward to obtain electron velocities within a self-consistent screening theory. Figure 4 shows electron velocities that flow through edge channels which are on the order of  $10^7$  cm/s. This result is consistent with previous theoretical calculations [43].

Self-consistent screening calculations depending on the electron-electron interactions explained by the recent theoretical works show that the 2DEG contains two different kinds of regions: the compressible and incompressible [44,45]. In the compressible region a partially filled LL with its high density of states is pinned to the Fermi energy and the electronic system behaves like a quasimetal and screens completely the confining potential. In contrast to the compressible region, when the Fermi level is between two consequent LLs, electrons do not contribute to screening locally; i.e., the confining potential could not be screened perfectly. Here, the system presents a constant electron density and is called “incompressible,” behaving like a quasi-insulator.

In a 2DEG the incompressibility is defined as

$$\kappa^{-1} = -S \left( \frac{\partial P}{\partial S} \right)_N = S \left( \frac{\partial^2 E}{\partial S^2} \right)_N, \quad (8)$$

where the pressure  $P = (\partial E / \partial S)$  is the change of energy according to the area change,  $S$  is the area of the 2DEG,  $N = S n_{\text{el}}$  is the total number of the electrons, and the total energy of the system is  $N$  times the ground state energy per particle,  $E_{\text{tot}} = N \varepsilon(n_{\text{el}})$ . Using standard manipulations, we may rewrite incompressibility according to changing the chemical potential instead of changing the electron number

density as

$$\kappa^{-1} = n_{\text{el}}^2 \left( \frac{d\mu}{dn_{\text{el}}} \right), \quad (9)$$

where the chemical potential  $\mu$  is related to the total energy  $E_{\text{tot}}$  by

$$\mu = \frac{\partial E_{\text{tot}}}{\partial N} = \frac{\partial (E_{\text{tot}}/S)}{\partial n_{\text{el}}}. \quad (10)$$

From Eq. (9) we can tell that the system is incompressible if the chemical potential increases discontinuously as a function of density. The incompressibility of the 2DEG is a fundamental thermodynamic quantity and proportional to the thermodynamical density of states (TDOS),  $D_T(\mu, B) = dn_{\text{el}}/d\mu$ , which is the rate of change of the chemical potential with electron concentration. To illustrate the meaning of the term thermodynamic density of states, we calculate

$$\frac{dn_{\text{el}}}{d\mu} = \frac{d}{d\mu} \int dE D(E) f(E) = \int dE D(E) \frac{df(E)}{d\mu}. \quad (11)$$

The TDOS tells us how much the ground state energy changes when an additional particle is added to the system [21].

#### IV. RESULTS

Utilizing the confinement potential obtained via solving the Poisson equation in 3D, we calculate the corresponding electron density distribution within the QD. Figure 5 depicts the spin densities for a QD that contains 30 electrons at the  $\nu = \frac{5}{2}$  state. Our numerical investigations show that the position of the incompressible strips and electron numbers in the second lowest LL differ from the results of the symmetric quantum Hall devices. Although the position of the incompressible strip shifts to the right side while applying  $-1.8$  V and  $-2.0$  V to the metallic gate, it shifts to the left side for  $-2.9$  V. Even so, it looks nearly symmetric when the metallic gate is biased with  $-2.3$  V. The electron numbers in the SD are 3, 4, 4, 5 for  $-1.8$  V,  $-2.0$  V,  $-2.3$  V,  $-2.9$  V, respectively.

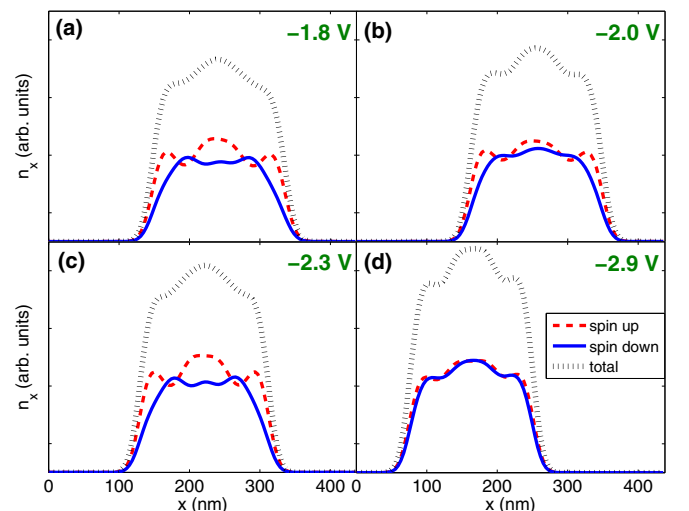


FIG. 5. Spin-up, spin-down, and total electron density of quantum Hall state in a QD includes 30 electrons calculated with the SDFT at  $\nu = \frac{5}{2}$  for various gate voltages.



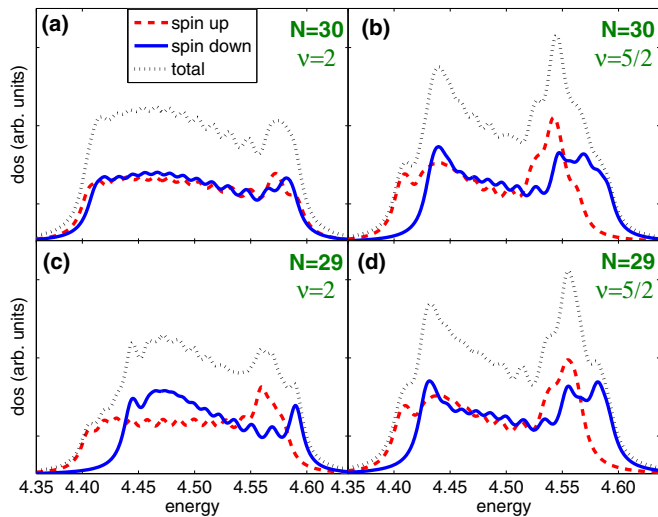


FIG. 6. LDOS for different electron numbers and filling factors.

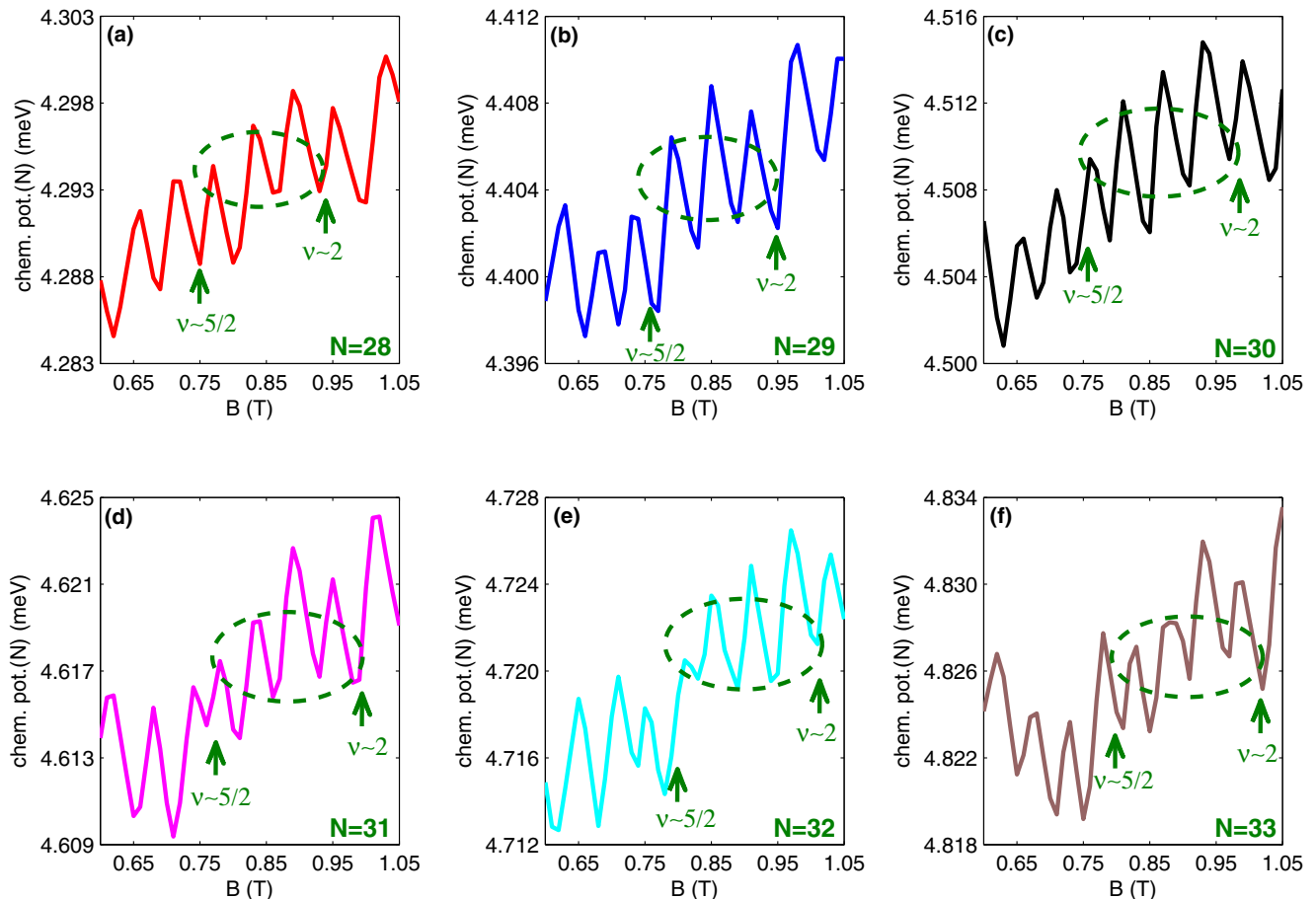
To check spin dependency of the spin droplet we obtain the local density of states (LDOS) when the total electron number is  $N = 30$  and  $N = 29$  inside the quantum dot for filling factor  $\nu = 2$  and  $\nu = \frac{5}{2}$ . Figure 6 shows LDOS for  $\nu = 2$  and  $\nu = \frac{5}{2}$ . We see that there is a peak in both 30 electrons

and 29 electrons for  $\nu = \frac{5}{2}$  and this indicates the presence of the spin droplet, incompressible droplets of spin-polarized second Landau level (SLL) electrons. The spin splitting of the SLL is analogous to the Stoner criterion [46], which states the presence of correlations between electrons with the same spin and high density of states near the Fermi level. Now, the system favors ferromagnetic alignment that reduces the degeneracy.

We discuss the consistency of finite-size counterparts of the integer and fractional quantum Hall states in the quantum dot which gives characteristic properties in the chemical potential. The existence and the properties of these states can be defined by chemical potential  $\mu(N, B) = E_{\text{tot}}(N, B) - E_{\text{tot}}(N - 1, B)$ , which is the energy needed to add the  $N$ th electron in the system of  $N - 1$  electrons. Figures 7 and 8 show results for chemical potentials in the comparison with various electron numbers for symmetric and asymmetric potentials, respectively. Sudden jumps in oscillations correspond to filling factor  $\nu = \frac{5}{2}$ . The observed jumps clearly indicate that the  $\frac{5}{2}$  state is compressible, once again regardless of the symmetry of the confinement.

## V. SUMMARY

In conclusion, we have seen the electronic compressibility of a 2DEG in the fractional quantum Hall regime. The compressibility images show a quasi-insulating region of


 FIG. 7. Chemical potentials compared with symmetric confining potential for various  $N$ -electron symmetric quantum dots as a function of the magnetic field  $B$ . The dotted ellipse denotes the spin-droplet regime.

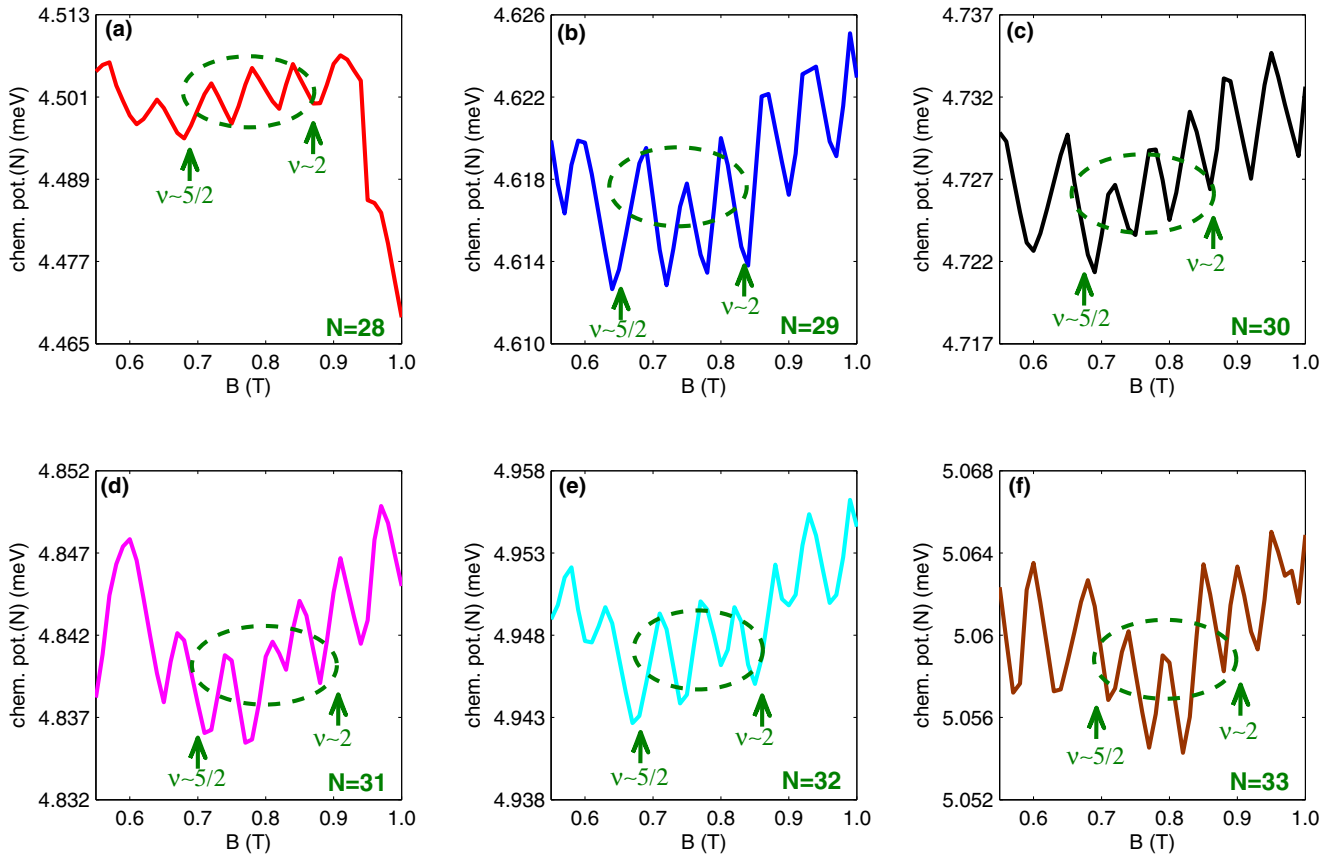


FIG. 8. Chemical potentials compared with asymmetric confining potential for various  $N$ -electron symmetric quantum dots as a function of the magnetic field  $B$ . The dotted ellipse denotes the spin-droplet regime.

electron liquid from near-integer filling. The incompressible strips form near the boundary of the sample due to a smooth density gradient. A potential step accompanies the incompressible strip. We see that the incompressibility of the filling factor  $\nu = \frac{5}{2}$  is strongly affected by the asymmetry of the potential of the sample. These findings are similar

to previous observation, even if the confinement potential is no longer asymmetric. Such a stable configuration of the spin droplet state also enables us to claim that this state is universal. Our numerical investigations also show that the position of the incompressible strips and electron numbers in the SLL differ from the results of the symmetric quantum Hall devices. Our calculations indicate that the paired electron

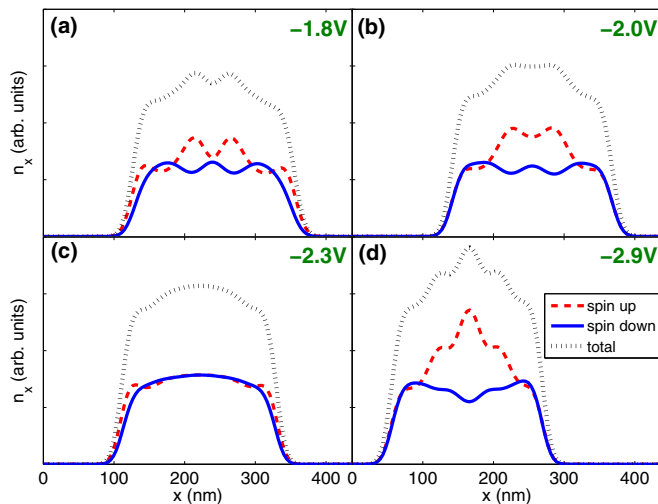


FIG. 9. Spin-up, spin-down, and total electron density of quantum Hall state in a QD that includes 48 electrons calculated with the SDFT at  $\nu = \frac{5}{2}$  for various gate voltages.

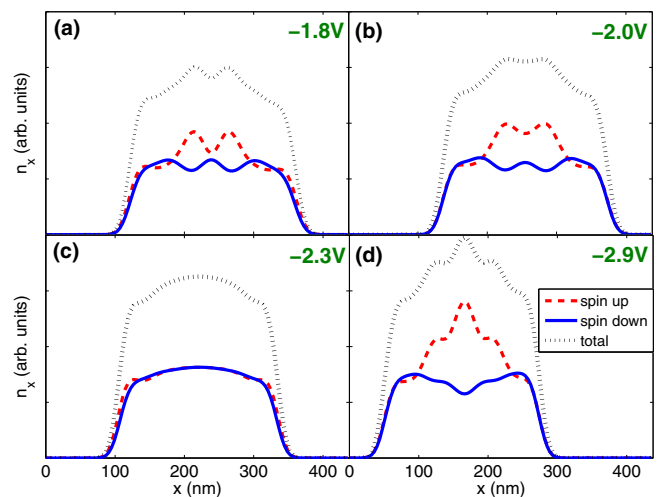


FIG. 10. Spin-up, spin-down, and total electron density of quantum Hall state in a QD that includes 54 electrons calculated with the SDFT at  $\nu = \frac{5}{2}$  for various gate voltages.

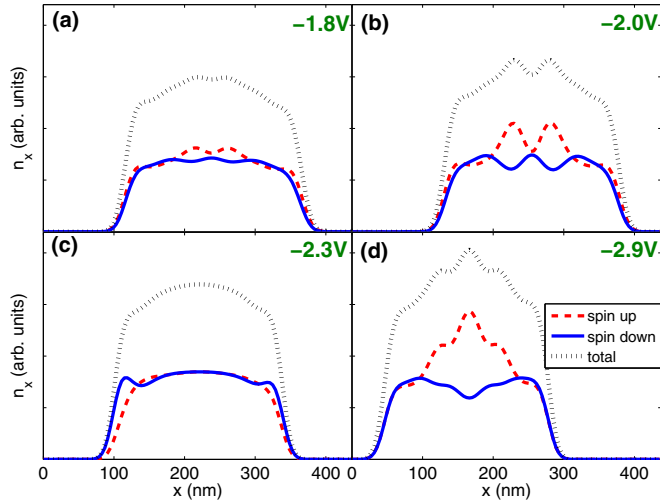


FIG. 11. Spin-up, spin-down, and total electron density of quantum Hall state in a QD that includes 60 electrons calculated with the SDFT at  $\nu = \frac{5}{2}$  for various gate voltages.

state breaks down leading to fragmentation of spin densities. We find evidence of fragmentation in several calculations but point out that our results can be tested by direct measurements of the spatial dependence of spin densities in different geometries and experimental setups. An asymmetric slope gives electron velocity and an electron with the order of  $10^7$  cm/s passes through interferometers. This result is consistent with previous theoretical calculations. It is concluded that the electron velocity is an important transport parameter for the interferometers.

It is essential to note that we do not claim that our model gives a complete picture of the  $\frac{5}{2}$  state for macroscopic devices. However, given the experimentally consistent reports, we think that experimentalists can perform detailed investigations on such asymmetric samples not only by device imperfectness but also controllably, utilizing electrostatic means.

#### ACKNOWLEDGMENTS

The authors would like to acknowledge the Scientific and Technical Research Council of Turkey (TUBITAK) for support under Grants No. 112T264 and No. 211T148, and Marmaris Institute of Theoretical and Applied Physics (ITAP). H.A.

TABLE I. Radii, densities, and numbers of electrons.

$R$ (nm)	$n_{el}$ ( $10^{-15} \text{ m}^{-2}$ )	$N$
440	0.9	135
440	1.2	180
390	0.9	107
390	1.2	143
220	0.9	34
220	1.2	45

also acknowledges support from TUBITAK under Grant No. 2214/A.

#### APPENDIX

In this appendix we would like to clarify a couple of issues related to the geometry and limited number of particles. First, as shown in Table I the parameter  $N$  we considered in the main text is still in the thermodynamic limit. We also performed similar calculations regarding a larger number of particles, which we present here.

Only considering the lithographic dimensions of the QD ( $R \sim 440$  nm) is rather unrealistic to calculate the number of particles with this parameter. However, in experiments in which the electrostatic repulsion is due to the trapping metallic gates, electrons are depleted from the edges, reducing the effective radius to  $\sim 220$  nm. Essentially, this can be clearly seen from Fig. 5 of our paper. Performing back of envelope calculations with the given experimental bulk and dot electron densities together with the lithographic and electrostatic confinement radii, the numbers of electrons are shown in Table I.

Given the numbers above we can say that our calculations considering 30 electrons are reasonably close to the experimental data. However, we also performed similar calculations considering 48, 54, and 60 electrons (cf. Figs. 9, 10, and 11, respectively). We observe that for 48 and 54 particles, the density distribution at  $\frac{5}{2}$  filling does not show any remarkable difference compared to 30 particles. For 60 particles, besides some variations at  $n_{el}(x)$  the general behavior, i.e., formation of the spin droplet and incompressible strips, is preserved. This result is also consistent with our previous work [17], where the potential is assumed to be symmetric. Hence, in this paper we have shown that, even if the confining potential is asymmetric (describing experiments realistically), one can obtain spin droplets.

- [1] R. Willett, J. P. Eisenstein, H. L. Stormer, D. C. Tsui, A. C. Gossard, and J. H. English, *Phys. Rev. Lett.* **59**, 1776 (1987).
- [2] C. R. Dean, B. A. Piot, P. Hayden, S. Das Sarma, G. Gervais, L. N. Pfeiffer, and K. W. West, *Phys. Rev. Lett.* **100**, 146803 (2008).
- [3] H. C. Choi, W. Kang, S. Das Sarma, L. N. Pfeiffer, and K. W. West, *Phys. Rev. B* **77**, 081301(R) (2008).
- [4] J. Xia, V. Cvicek, J. P. Eisenstein, L. N. Pfeiffer, and K. W. West, *Phys. Rev. Lett.* **105**, 176807 (2010).
- [5] J. Shabani, Y. Liu, and M. Shayegan, *Phys. Rev. Lett.* **105**, 246805 (2010).
- [6] W. Pan, N. Masuhara, N. S. Sullivan, K. W. Baldwin, K. W. West, L. N. Pfeiffer, and D. C. Tsui, *Phys. Rev. Lett.* **106**, 206806 (2011).
- [7] M. R. Peterson, T. Jolicoeur, and S. Das Sarma, *Phys. Rev. B* **78**, 155308 (2008).
- [8] M. R. Peterson, T. Jolicoeur, and S. Das Sarma, *Phys. Rev. Lett.* **101**, 016807 (2008).

- [9] A. Wojs, C. Toke, and J. K. Jain, *Phys. Rev. Lett.* **105**, 096802 (2010).
- [10] C. Nayak, S. H. Simon, A. Stern, M. Freedman, and S. Das Sarma, *Rev. Mod. Phys.* **80**, 1083 (2008).
- [11] G. Moore and N. Read, *Nucl. Phys. B* **360**, 362 (1991).
- [12] S. Das Sarma, M. Freedman, and C. Nayak, *Phys. Rev. Lett.* **94**, 166802 (2005).
- [13] A. Stern and B. I. Halperin, *Phys. Rev. Lett.* **96**, 016802 (2006).
- [14] W. Bishara and C. Nayak, *Phys. Rev. B* **77**, 165302 (2008).
- [15] S. Baer, C. Rössler, T. Ihn, K. Ensslin, C. Reichl, and W. Wegscheider, *New J. Phys.* **15**, 023035 (2013).
- [16] E. Räsänen, H. Saarikoski, A. Harju, M. Ciorga, and A. S. Sachrajda, *Phys. Rev. B* **77**, 041302(R) (2008).
- [17] H. Atci, U. Erkarlan, A. Siddiki, and E. Rasanen, *J. Phys.: Condens. Matter* **25**, 155604 (2013).
- [18] B. Rosenow, B. I. Halperin, S. H. Simon, and A. Stern, *Phys. Rev. B* **80**, 155305 (2009).
- [19] A. Harju, H. Saarikoski, and E. Rasanen, *Phys. Rev. Lett.* **96**, 126805 (2006).
- [20] H. Saarikoski, E. Tolo, A. Harju, and E. Rasanen, *Phys. Rev. B* **78**, 195321 (2008).
- [21] Z. F. Ezawa, *Quantum Hall Effects: Field Theoretical Approach and Related Topics*, 2nd ed. (World Scientific Publishing Company, 2008).
- [22] F. E. Camino, W. Zhou, and V. J. Goldman, *Phys. Rev. B* **72**, 155313 (2005).
- [23] F. E. Camino, W. Zhou, and V. J. Goldman, *Phys. Rev. Lett.* **98**, 076805 (2007).
- [24] A. Siddiki and R. R. Gerhardts, *Phys. Rev. B* **68**, 125315 (2003).
- [25] A. Siddiki and R. R. Gerhardts, *Phys. Rev. B* **70**, 195335 (2004).
- [26] J. H. Oh and R. R. Gerhardts, *Phys. Rev. B* **56**, 13519 (1997).
- [27] K. Guven and R. R. Gerhardts, *Phys. Rev. B* **67**, 115327 (2003).
- [28] P. M. Morse and H. Feshbach, *Methods of Theoretical Physics* (McGraw-Hill, New York, 1953).
- [29] S. Arslan, E. Cicek, D. Eksi, S. Aktas, A. Weichselbaum, and A. Siddiki, *Phys. Rev. B* **78**, 125423 (2008).
- [30] A. I. Mese, A. Bilekkaya, S. Arslan, S. Aktas, and A. Siddiki, *J. Phys. A: Math. Theor.* **43**, 354017 (2010).
- [31] A. Weichselbaum and S. E. Ulloa, *Phys. Rev. E* **68**, 056707 (2003).
- [32] A. Weichselbaum and S. E. Ulloa, *Phys. Rev. B* **74**, 085318 (2006).
- [33] M. C. Rogge, E. Rasanen, and R. J. Haug, *Phys. Rev. Lett.* **105**, 046802 (2010).
- [34] F. E. Camino, W. Zhou, and V. J. Goldman, *Phys. Rev. B* **72**, 075342 (2005).
- [35] Y. Ji, Y. Chung, D. Sprinzak, M. Heiblum, D. Nahalu, and H. Shtrikman, *Nature (London)* **422**, 415 (2003).
- [36] D. T. McClure, Y. Zhang, B. Rosenow, E. M. Levenson-Falk, C. M. Marcus, L. N. Pfeiffer, and K. W. West, *Phys. Rev. Lett.* **103**, 206806 (2009).
- [37] W. Kohn and L. J. Sham, *Phys. Rev.* **140**, A1133 (1965).
- [38] U. von Barth and L. Hedin, *J. Phys. C* **5**, 1629 (1972).
- [39] C. Attaccalite, S. Moroni, P. Gori-Giorgi, and G. B. Bachelet, *Phys. Rev. Lett.* **88**, 256601 (2002).
- [40] M. A. L. Marques, A. Castro, G. F. Bertsch, and A. Rubio, *Comput. Phys. Commun.* **151**, 60 (2003).
- [41] A. Castro, H. Appel, M. Oliveira, C. A. Rozzi, X. Andrade, F. Lorenzen, M. A. L. Marques, E. K. U. Gross, and A. Rubio, *Phys. Status Solidi B* **243**, 2465 (2006).
- [42] For a review on density-functional theory, see, e.g., R. M. Dreizler and E. K. U. Gross, *Density Functional Theory* (Springer, Berlin, 1990).
- [43] D. Eksi, E. Cicek, A. I. Mese, S. Aktas, A. Siddiki, and T. Hakioglu, *Phys. Rev. B* **76**, 075334 (2007).
- [44] A. Siddiki and F. Marquardt, *Phys. Rev. B* **75**, 045325 (2007).
- [45] A. Salman, E. Koymen, M. B. Yucel, H. Atci, U. Erkarlan, and A. Siddiki, *Physica E* **44**, 1425 (2012).
- [46] E. C. Stoner, *Proc. R. Soc. London A* **165**, 372 (1938).